SAE TECHNICAL PAPER SERIES

2008-01-0517

Occupant Trajectory Model using Case-Specific Accident Reconstruction Data for Vehicle Position, Roll, and Yaw

Chad B. Hovey, Matthew L. Kaplan and Robert L. Piziali
Piziali and Associates, Iinc.

Reprinted From: Biomechanics, 2008 (SP-2163)

ISBN 978-0-7680-1631-4

**2008 World Congress
Detroit, Michigan
April 14-17, 2008**

SAE International™

400 Commonwealth Drive, Warrendale, PA 15096-0001 U.S.A. Tel: (724) 776-4841 Fax: (724) 776-0790 Web: www.sae.org

All SAE papers, standards, and selected books are abstracted and indexed in the Global Mobility Database.

ISSN 0148-7191

Printed in USA

2008-01-0517

Occupant Trajectory Model using Case-Specific Accident Reconstruction Data for Vehicle Position, Roll, and Yaw

Chad B. Hovey, Matthew L. Kaplan and Robert L. Piziali
Piziali and Associates, Inc.

ABSTRACT

In the fields of accident reconstruction and injury biomechanics, it is often of interest to know details of an occupant's ejection from a vehicle during a rollover. Current occupant trajectory models do not account for vehicle yaw and yaw rate. Such considerations are compulsory if the occupant's rest point has a non-trivial deviation from the vehicle's roll path. Moreover, many existing models use a single, generic function for the roll rate for all analyses. Such approaches intrinsically model all rollovers as identical events, regardless of the underlying uniqueness a particular accident may exhibit.

The objective of this work is to model the trajectory of an occupant ejected from a vehicle in a rollover event. In particular, we model the vehicle's longitude, latitude, roll, yaw, and time derivatives thereof, based on data extracted from a particular accident reconstruction. We model the occupant moving in the vehicle and possibly ejected at any time during the rollover. For each admissible ejection time, we construct an occupant trajectory, landing point, and point of rest (POR). We illustrate the effectiveness of our model with a case-study where significant yaw occurs during the rollover.

Our new model, when compared with existing approaches, provides an improved understanding of occupant ejection. Additionally, the new model eliminates spurious ejection solutions predicted by previous formulations. Finally, the new model is tailored to the underlying accident reconstruction data, producing a simulation that is based on the uniqueness of a particular rollover event.

INTRODUCTION

The vehicle dynamics of rollovers has been studied by numerous researchers in the absence of consideration of the occupants [Carter, 2002; Cooperrider, 1998; Thomas, 1989]. Others have examined the kinematics of occupants in rollover accidents, but have not modeled ejections of occupants [Orlowski, 1985; Parenteau, 2001]. Occupant trajectories have been researched in the context of pedestrian-vehicle impacts and motorcycle accidents [Aronberg, 1990; Searle, 1983; Searle, 1993; Wood, 1991]. These models apply to the airborne phase and sliding phase of a particle, and determine the launch velocity with a known total distance from launch to point of rest. In the context of rollover accidents, the launch velocity can be calculated as a function of vehicle and occupant kinematics, however, the time and vehicle location when the occupant is ejected is unknown. It is useful to predict when in the roll sequence an ejection occurred to understand details of the injury biomechanics, such as how far the occupant was thrown from the vehicle, or if there was post-ejection vehicle-ejectee contact.

A successful model of occupant ejection in rollover accidents incorporates the reconstruction information with the occupant's point of rest to determine the time of ejection, the ejection velocity, and subsequent trajectory. Funk and Luepke have published a model of occupant ejection in rollovers [Funk, 2007]. This model includes the vehicle dynamics in the longitudinal direction and takes into account roll angle and roll rate. Rather than use case-specific data for the vehicle roll angle and roll rate, Funk and Luepke assume a prescribed functional form, while noting other roll functions could be used. Their model does not consider yaw effects or lateral distance to the occupant's point of rest.

Previous published occupant trajectory formulations lack the inclusion of roll and yaw data derived from a case-specific accident reconstruction. Moreover, these models predict possible ejection points based solely on a trajectory that is along the vehicle's longitudinal roll path. Solv-

ing for the possible ejection times in the longitudinal direction produces a set of possible ejection points. These ejection points are not all feasible, however, when the vehicle does not have linear roll path, when the vehicle has non-trivial yaw characteristics, or when the occupant's point of rest deviates from the path of the vehicle. By incorporating the yaw effects, the set of predicted solutions can be pared down to a subset of solutions that matches the point of rest in both the longitudinal and lateral directions.

Extending on our previous work [Hovey, 2007], the objective of this work is to develop a comprehensive model for occupant trajectories following ejections in rollover accidents. This model uses case-specific reconstruction data to determine candidate ejection times and the corresponding ejection velocities and trajectories of the ejectee.

METHODS

The occupant trajectory model is composed of a vehicle model and an occupant model. The vehicle model describes the motion of the vehicle from its point of trip to point of rest. From trip to rest, the vehicle translates longitudinally and laterally in the ground plane, and rotates with roll and yaw. During the rollover, the occupant is initially in the vehicle, is ejected from the vehicle, moves through the air free from the vehicle, lands on the ground, and comes to rest. The occupant model describes the motion of the occupant throughout three phases: (1) moving within the vehicle, (2) moving through the air, (3) moving on the ground.

VEHICLE MODEL The vehicle is modeled as a body that translates, rolls, and yaws in the ground plane. For the present formulation, changes in elevation of the ground plane and vehicle are ignored. Vehicle rotation along the pitch axis is also ignored.

Reference Frames Let the inertial reference frame $\mathcal{F}$ have unit vectors $[\hat{e}_{\mathcal{F}1}, \hat{e}_{\mathcal{F}2}, \hat{e}_{\mathcal{F}3}]$ at origin F. Unit vector $\hat{e}_{\mathcal{F}1}$ points down the roadway in the vehicle's approximate direction of travel prior to the rollover event. Unit vector $\hat{e}_{\mathcal{F}2}$ points laterally to the left of the direction of travel, in the plane of travel. Unit vector $\hat{e}_{\mathcal{F}3}$ points up from and is perpendicular to the plane of travel. All unit vectors used in this paper are dextral, orthonormal, ordered triads.

Let the carrier frame $\mathcal{C}$ be attached to the vehicle's center of mass at point V. The carrier frame has unit vectors $[\hat{e}_{\mathcal{C}1}, \hat{e}_{\mathcal{C}2}, \hat{e}_{\mathcal{C}3}]$. Unit vector $\hat{e}_{\mathcal{C}1}$ points toward the front of the vehicle. Unit vector $\hat{e}_{\mathcal{C}2}$ points to the left of the vehicle, with the vehicle in a non-rolling configuration. Unit vector $\hat{e}_{\mathcal{C}3}$ points to the roof of the vehicle, with the vehicle in a non-rolling configuration. Note that the carrier frame is not attached to the vehicle and thus does not roll with the vehicle. The carrier frame rotates with the yaw of the vehicle with respect to the inertial frame along the vertical axis.

Let the vehicle frame $\mathcal{V}$ be fixed to the vehicle's center of mass at point V. The vehicle's frame has unit vectors $[\hat{e}_{\mathcal{V}1}, \hat{e}_{\mathcal{V}2}, \hat{e}_{\mathcal{V}3}]$. Unit vector $\hat{e}_{\mathcal{V}1}$ points to the front of the vehicle. Unit vector $\hat{e}_{\mathcal{V}2}$ points to the left of the vehicle. Unit vector $\hat{e}_{\mathcal{V}3}$ points to the roof of the vehicle.

Fig. 1 illustrates these reference frames. Note that this convention differs from the SAE convention.

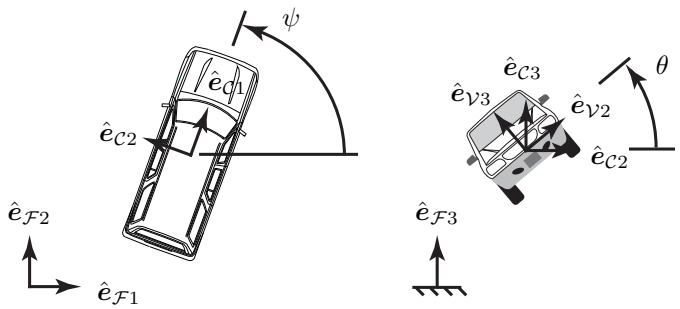

Figure 1: Illustration of inertial, carrier, and vehicle reference frames in a top view (left subfigure) and vehicle front view (right subfigure).

Degrees of Freedom The vehicle translates in the inertial frame as ${}^{\mathcal{F}}\boldsymbol{r}^{FV} = x\,\hat{\boldsymbol{e}}_{\mathcal{F}1} + y\,\hat{\boldsymbol{e}}_{\mathcal{F}2} + z\,\hat{\boldsymbol{e}}_{\mathcal{F}3}$. The $\{x, y, z\}$ triad corresponds to the vehicle's longitude, latitude, and elevation at any time. Since we ignore elevation changes, z is constant for all time.

The carrier frame $\mathcal{C}$ rotates with respect to the inertial reference frame about the $\hat{e}_{\mathcal{C}3}$ axis, which is coincident with the $\hat{e}_{\mathcal{F}3}$ axis for all time. This rotation, ψ, represents the yaw angle of the vehicle. As viewed from above the vehicle, a positive ψ is a counterclockwise yaw; a negative ψ is a clockwise yaw.

The vehicle frame $\mathcal{V}$ rotates with respect to the carrier frame $\mathcal{C}$ about the $\hat{e}_{\mathcal{V}1}$ axis, which is coincident with the $\hat{e}_{\mathcal{C}1}$ axis for all time. This rotation, θ, represents the roll angle of the vehicle. A positive θ is a right-side-leading roll; a negative θ is a left-side-leading roll. For vehicles with the steering wheel on the left side of the vehicle, this convention extends to be a passenger-side-leading roll (positive roll angle) and a driver-side-leading roll (negative roll angle), respectively.

Initial Conditions We consider the point of trip to be the initial time $t = 0$. At the initial time, the vehicle's position and orientation are known from the accident reconstruction, written explicitly as $\{x_0, y_0, z_0, \psi_0, \theta_0\}$.

Determination of $\dot{x}_0$ and $\dot{y}_0$ requires consideration of the vehicle's path during the rollover. The vehicle translates from its point of trip to its point of rest along a path, defined as ${}^{\mathcal{F}}\boldsymbol{s}^{V}$. The path from trip to rest may not be linear,

and generally may have arcing or serpentine shapes. The length of the roll path, $\| \int d\boldsymbol{s} \|$, is often referred to as the roll distance. We denote the roll distance as Δs, bearing in mind the roll distance is path-dependent. The roll distance is a known quantity, obtained from the accident reconstruction.

From conservation of energy, we find the vehicle's initial speed, $\dot{s}_0$, as

$$\dot{s}_0 = \sqrt{2\mu g \Delta s}, \tag{1}$$

where μ is the drag factor, assumed to be a constant, and g is the gravitational constant. The initial speed is also called the trip speed. The present formulation assumes a flat roll plane, and thus potential energy contributions due to changes in elevation have been ignored.

The path angle, α, along which the vehicle translates in the plane can be found from the accident reconstruction. The path angle is measured from the global reference frame axis $\hat{\boldsymbol{e}}_{\mathcal{F}1}$ to the tangent of the path at any point along the path. A positive value of α makes a positive rotation along the $\hat{\boldsymbol{e}}_{\mathcal{F}3}$ axis; a negative value of α makes a negative rotation along the $\hat{\boldsymbol{e}}_{\mathcal{F}3}$ axis. To construct a continuous function for α, we interpolate piecewise linear functions of path lines connecting vehicle positions between templates on the accident reconstruction diagram.

With the path speed $\dot{s}$ and path angle α known for all time, the component speeds $\dot{x}$ and $\dot{y}$ can be expressed as $\dot{x} = \dot{s}\cos(\alpha)$ and $\dot{y} = \dot{s}\sin(\alpha)$. The initial conditions, $\dot{x}_0$ and $\dot{y}_0$, are then expressed at $t = 0$ with $\dot{s}_0$ and α_0. Since z is assumed constant for all time, $\dot{z} = 0$ for all time and thus $\dot{z}_0 = 0$.

The initial conditions for $\dot{\psi}_0$ and $\dot{\theta}_0$ can be estimated from the accident reconstruction. Some accident reconstructionists define the trip point at $\theta_0 = 0$, for which taking $\dot{\theta}_0 = 0$ is reasonable. Other accident reconstructionists define the trip point at $\theta_0 = \pm\pi/8$, for which a non-zero input for $\dot{\theta}_0$ may be appropriate.

Equations of Motion The governing equation of motion along the vehicle's path is given by

$$\ddot{s} = -\mu g, \tag{2}$$

where $\ddot{s}$ is the vehicle's acceleration along the path.

Integrating the governing equation of motion from the time when the vehicle trips, t_0, to the time when the vehicle comes to rest, t_f, gives the roll time, Δt_{roll}, where

$$\Delta t_{\text{roll}} = \frac{\dot{s}_0}{\mu g}. \tag{3}$$

The vehicle's speed along the path at any time is given by

$$\dot{s}_t = \dot{s}_0 - \mu g t, \quad \forall\, t \in [t_0, t_f]. \tag{4}$$

The vehicle's distance along the path at any time is given by

$$s_t = \dot{s}_0 t - \frac{1}{2}\mu g t^2, \quad \forall\, t \in [t_0, t_f]. \tag{5}$$

The vehicle's component speeds are then given by

$$\dot{x}_t = \dot{s}_t \cos\alpha_t, \tag{6}$$

$$\dot{y}_t = \dot{s}_t \sin\alpha_t. \tag{7}$$

The vehicle's x and y positions must be integrated along the path

$$x_t = \int_{t_0}^{t} \hat{\boldsymbol{e}}_{\mathcal{F}1} \cdot d\dot{\boldsymbol{s}}, \tag{8}$$

$$y_t = \int_{t_0}^{t} \hat{\boldsymbol{e}}_{\mathcal{F}2} \cdot d\dot{\boldsymbol{s}}. \tag{9}$$

The vehicle's yaw angle ψ and roll angle θ are interpolated similarly to the vehicle's path angle α. From the accident reconstruction, the roll and yaw angles are extracted for every vehicle template between and including the point of trip and point of rest. Piecewise linear functions are interpolated between known yaw and roll angles at each of the vehicle template locations.

Yaw rates and roll rates are constructed in a similar manner. For a given template, the yaw angle at the current template, minus the yaw angle from the previous template, divided by the time elapsed between the current and previous template, is calculated to give the yaw rate at the current template. The discrete yaw rates at each template are then used to construct piecewise linear functions, providing an interpolation for the yaw rate $\dot{\psi}$.

Roll rates are constructed in an exactly analogous manner and may include the following modification. To satisfy the constraint that the roll rate, integrated over time, must be equal to the number of rolls, n_{rolls}, we introduce a roll rate scaling κ such that

$$360^\circ \cdot n_{\text{rolls}} = \int_{t_0}^{t_f} \kappa\, \dot{\theta}\, dt, \tag{10}$$

to calculate a consistent roll rate.

OCCUPANT MODEL The occupant model includes three phases: (1) the occupant moving within the vehicle, (2) the occupant being ejected and moving through the air, and (3) the occupant landing on the ground and coming to rest. The occupant is modeled as a point mass with three translational degrees of freedom.

Occupant in Vehicle Let an occupant be located at point O, moving in the vehicle frame $\mathcal{V}$. The occupant is located with respect the vehicle as

$${}^{\mathcal{V}}\boldsymbol{r}^{VO} = \chi\, \hat{\boldsymbol{e}}_{\mathcal{V}1} + \rho\cos\phi\, \hat{\boldsymbol{e}}_{\mathcal{V}2} + \rho\sin\phi\, \hat{\boldsymbol{e}}_{\mathcal{V}3}, \tag{11}$$

where ϕ is an angle in the $[\hat{e}_{\mathcal{V}2}, \hat{e}_{\mathcal{V}3}]$ plane. The occupant is assumed to have non-trivial velocities within the vehicle frame in the longitudinal and radial directions, and zero velocities in the tangential direction, thus

$$ {}^{\mathcal{V}}\boldsymbol{v}^{O} = \left\{ \begin{array}{c} \dot{\chi} \\ \dot{\rho}\cos\phi \\ \dot{\rho}\sin\phi \end{array} \right\}. \tag{12} $$

The velocity of the occupant expressed in the inertial frame $\mathcal{F}$ is given by

$$ {}^{\mathcal{F}}\boldsymbol{v}^{O} = {}^{\mathcal{F}}\boldsymbol{v}^{V} + {}^{\mathcal{V}}\boldsymbol{v}^{O} + {}^{\mathcal{F}}\boldsymbol{\omega}^{\mathcal{V}} \times \boldsymbol{r}^{VO}, \tag{13} $$

where ${}^{\mathcal{F}}\boldsymbol{v}^{V}$ is the velocity of the vehicle relative to the inertial frame, ${}^{\mathcal{V}}\boldsymbol{v}^{O}$ is the velocity of the occupant relative to the vehicle frame, ${}^{\mathcal{F}}\boldsymbol{\omega}^{\mathcal{V}}$ is the angular velocity of the vehicle in the inertial frame, and $\boldsymbol{r}^{VO}$ is the position vector from the vehicle at point V to the occupant at point O.

Considering each of these terms successively, we have

$$ {}^{\mathcal{F}}\boldsymbol{v}^{V} = \left\{ \begin{array}{c} \dot{x} \\ \dot{y} \\ \dot{z} \end{array} \right\}, \tag{14} $$

which is simply the translational speed of the vehicle. The velocity ${}^{\mathcal{V}}\boldsymbol{v}^{O}$ in the inertial reference frame is given by ${}^{\mathcal{F}}\tilde{\boldsymbol{v}}^{O} = {}^{\mathcal{F}}\boldsymbol{Q}^{\mathcal{V}} \cdot {}^{\mathcal{V}}\boldsymbol{v}^{O}$, or explicitly by

$$ {}^{\mathcal{F}}\tilde{\boldsymbol{v}}^{O} = \left\{ \begin{array}{c} \dot{\chi}\cos\psi - \dot{\rho}\sin\psi\,(\cos\theta\cos\phi - \sin\theta\sin\phi) \\ \dot{\chi}\sin\psi + \dot{\rho}\cos\psi\,(\cos\theta\cos\phi - \sin\theta\sin\phi) \\ \dot{\rho}\,(\sin\theta\cos\phi + \cos\theta\sin\phi) \end{array} \right\}, \tag{15} $$

where

$$ \dot{\chi} = {}^{\mathcal{V}}\boldsymbol{v}^{O} \cdot \hat{\boldsymbol{e}}_{\mathcal{V}1}, \tag{16} $$

where

$$ \dot{\rho} = \sqrt{({}^{\mathcal{V}}\boldsymbol{v}^{O} \cdot \hat{\boldsymbol{e}}_{\mathcal{V}2})^2 + ({}^{\mathcal{V}}\boldsymbol{v}^{O} \cdot \hat{\boldsymbol{e}}_{\mathcal{V}3})^2}, \tag{17} $$

and where the transformation matrix from the vehicle to inertial reference frame, ${}^{\mathcal{F}}\boldsymbol{Q}^{\mathcal{V}} = {}^{\mathcal{F}}\boldsymbol{Q}^{\mathcal{C}} \cdot {}^{\mathcal{C}}\boldsymbol{Q}^{\mathcal{V}}$, has been used, viz.,

$$ {}^{\mathcal{F}}\boldsymbol{Q}^{\mathcal{V}} = \left[\begin{array}{ccc} \cos\psi & -\sin\psi\cos\theta & \sin\psi\sin\theta \\ \sin\psi & \cos\psi\cos\theta & -\cos\psi\sin\theta \\ 0 & \sin\theta & \cos\theta \end{array} \right]. \tag{18} $$

The value $\dot{\chi}$ is the speed of the occupant in the frame of the vehicle in the longitudinal direction of the vehicle (moving toward either the front or the rear of the vehicle). The value $\dot{\rho}$ is the speed of the occupant in the frame of the vehicle in the radial direction, co-planar with the vehicle's roll plane spanned by $[\hat{e}_{\mathcal{V}2}, \hat{e}_{\mathcal{V}3}]$.

The final term in Eq. (13), expressed in $\mathcal{F}$, is given by

$$ {}^{\mathcal{F}}\boldsymbol{\omega}^{\mathcal{V}} \times \boldsymbol{r}^{VO} = \left\{ \begin{array}{c} \sin\psi\,\dot{\theta}\,\xi_3 - \dot{\psi}\,\xi_2 \\ -\cos\psi\,\dot{\theta}\,\xi_3 + \dot{\psi}\,\xi_1 \\ \cos\psi\,\dot{\theta}\,\xi_2 - \sin\psi\,\dot{\theta}\,\xi_1 \end{array} \right\}, \tag{19} $$

where the explicit form for $\boldsymbol{r}^{VO}$ expressed in the reference from $\mathcal{F}$ is given by ${}^{\mathcal{F}}\boldsymbol{r}^{VO} = \{\xi_1, \xi_2, \xi_3\}^T$, or

$$ \left\{ \begin{array}{c} \xi_1 \\ \xi_2 \\ \xi_3 \end{array} \right\} = \left\{ \begin{array}{c} \chi\cos\psi - \rho\sin\psi\,(\cos\theta\cos\phi - \sin\theta\sin\phi) \\ \chi\sin\psi + \rho\cos\psi\,(\cos\theta\cos\phi - \sin\theta\sin\phi) \\ \rho\,(\sin\theta\cos\phi + \cos\theta\sin\phi) \end{array} \right\} \tag{20} $$

with

$$ \chi = {}^{\mathcal{V}}\boldsymbol{r}^{VO} \cdot \hat{\boldsymbol{e}}_{\mathcal{V}1}, \tag{21} $$

$$ \rho = \sqrt{({}^{\mathcal{V}}\boldsymbol{r}^{VO} \cdot \hat{\boldsymbol{e}}_{\mathcal{V}2})^2 + ({}^{\mathcal{V}}\boldsymbol{r}^{VO} \cdot \hat{\boldsymbol{e}}_{\mathcal{V}3})^2}, \tag{22} $$

and where the angular velocity vector is ${}^{\mathcal{F}}\boldsymbol{\omega}^{\mathcal{V}} = {}^{\mathcal{F}}\boldsymbol{\omega}^{\mathcal{C}} + {}^{\mathcal{C}}\boldsymbol{\omega}^{\mathcal{V}}$, or explicitly,

$$ {}^{\mathcal{F}}\boldsymbol{\omega}^{\mathcal{V}} = \left\{ \begin{array}{c} \cos\psi\,\dot{\theta} \\ \sin\psi\,\dot{\theta} \\ \dot{\psi} \end{array} \right\}. \tag{23} $$

Occupant in Air The air phase begins with the occupant's ejection from the vehicle and ends with the occupant's first impact with the ground. The governing equation of motion for the occupant is simply

$$ {}^{\mathcal{F}}\dot{\boldsymbol{v}}^{O} = -g\,\hat{\boldsymbol{e}}_{\mathcal{F}3}, \tag{24} $$

with initial conditions set as

$$ {}^{\mathcal{F}}\boldsymbol{v}^{O}_{\text{eject}} = {}^{\mathcal{F}}\boldsymbol{v}^{O}\big|_{t=t_{\text{eject}}}, \tag{25} $$

and

$$ {}^{\mathcal{F}}\boldsymbol{r}^{FO}_{\text{eject}} = {}^{\mathcal{F}}\boldsymbol{r}^{FO}\big|_{t=t_{\text{eject}}}. \tag{26} $$

For the ejection velocity, we decompose the components with respect to the vehicle frame as follows. We allow for a forward-aft velocity component, $\dot{\chi}$, along the $\hat{e}_{\mathcal{V}1}$ axis. We also allow for a radial velocity component, of magnitude $\dot{\rho}$. The velocity vector is written in Eq. (12). The value for $\dot{\chi}$ is often set to zero for rollover simulations, but is included in general to accommodate situations where ejections may occur via a rear or front window, as opposed to a side window or a sunroof. The value for $\dot{\rho}$ accounts for instances when the adjacent portal is blocked by the ground as the vehicle rolls. To construct the radial velocity component, we first compute the change in roll angle, $\Delta\theta_{\text{eject}}$, of the vehicle traversed during the ejection process within a particular vehicle roll. Let ϑ be the relative roll angle of the vehicle, such that $0 \le \vartheta \le 360°$. The relative roll angle is constructed simply for mathematical convenience, allowing the same functions to apply to any roll within the roll sequence. For a leading side ejection, we use

$$ \Delta\theta_{\text{eject, lead}} = \left\{ \begin{array}{cl} (\vartheta - 90)° & \text{for } 135° \le \vartheta \le 360°, \\ 0° & \text{otherwise.} \end{array} \right. \tag{27} $$

For a trailing side ejection, we use

$$ \Delta\theta_{\text{eject, trail}} = \left\{ \begin{array}{cl} (\vartheta + 90)° & \text{for } 0° \le \vartheta \le 180°, \\ (\vartheta - 270)° & \text{for } 315° \le \vartheta \le 360°, \\ 0° & \text{otherwise.} \end{array} \right. \tag{28} $$

We then compute the duration of the ejection time, Δt_{eject}, from the change in angle of the ejection, $\Delta\theta_{\text{eject}}$, divided

by the roll rate $\dot{\theta}$ when the vehicle is at a given roll angle θ, viz.,

$$\Delta t_{\text{eject}} = \frac{\Delta\theta_{\text{eject}}}{\dot{\theta}}. \tag{29}$$

We next set a distance, γ, the occupant travels within the vehicle during the ejection process, from their original seating configuration to their portal of ejection. We use the nominal value of $\gamma = 2$ feet, but this value to can tailored to any specific circumstance dictated by the vehicle's geometry. We calculate the radial speed the occupant would have if they are accelerated along the radial direction using the simple equation $\gamma = \frac{1}{2}\ddot{\gamma}t^2 + \dot{\gamma}_0 t + \gamma_0$ with $\dot{\gamma}_0 = \gamma_0 = 0$. Realizing this acceleration is strictly in the radial direction, we more conveniently note $\ddot{\gamma}$ as a_r, and solve

$$a_r = \frac{2\gamma}{\Delta t^2_{\text{eject}}}. \tag{30}$$

Next we calculate the maximum centripetal acceleration, $a_{r\,\max}$, the occupant could be experiencing due to the distance from the vehicle's roll center and the vehicle's roll rate as

$$a_{r\,\max} = \rho\,\dot{\theta}^2. \tag{31}$$

Since we know the actual occupant radial acceleration cannot exceed the maximum available radial acceleration, we solve for the radial speed,

$$\dot{\rho} = \begin{cases} a_r\,\Delta t_{\text{eject}} & \text{if } a_r < a_{r\,\max}\,, \\ a_{r\,\max}\,\Delta t_{\text{eject}} & \text{otherwise.} \end{cases} \tag{32}$$

The position vector to the occupant at ejection is found by using ${}^{\mathcal{F}}\boldsymbol{r}^{FO} = {}^{\mathcal{F}}\boldsymbol{r}^{FV} + {}^{\mathcal{F}}\boldsymbol{r}^{VO}$. Referencing Eq. (20) for ${}^{\mathcal{F}}\boldsymbol{r}^{VO}$, we write the position vector the occupant at ejection explicitly as

$${}^{\mathcal{F}}\boldsymbol{r}^{FO} = \begin{Bmatrix} x + \xi_1 \\ y + \xi_2 \\ z + \xi_3 \end{Bmatrix}. \tag{33}$$

The launch angle of the occupant at ejection, β^O_{eject}, can be considered from trigonometric considerations of the components of the occupant's velocity vector at ejection, ${}^{\mathcal{F}}\boldsymbol{v}^O_{\text{eject}}$. If the $\hat{\boldsymbol{e}}_{\mathcal{F}3}$ component of this vector is positive, the occupant is launched upward from the level plane; if it is negative, the occupant is launched downward toward the ground. This component is found from ${}^{\mathcal{F}}v^O_{z,\text{ eject}} = {}^{\mathcal{F}}\boldsymbol{v}^O_{\text{eject}} \cdot \hat{\boldsymbol{e}}_{\mathcal{F}3}$. In all cases, we determine occupant's maximum height, $h^O_{\max}$, vertical landing speed, ${}^{\mathcal{F}}v^O_{z,\text{ land}}$, and time in the air from launch to impact, Δt^O_{air}, as follows:
if $({}^{\mathcal{F}}v^O_{z,\text{ eject}} > 0)$ then

$$\begin{aligned} h^O_{\max} &= \boldsymbol{r}^{FO}_{\text{eject}} \cdot \hat{\boldsymbol{e}}_{\mathcal{F}3} + \frac{\left({}^{\mathcal{F}}v^O_{z,\text{ eject}}\right)^2}{2g}, \\ {}^{\mathcal{F}}v^O_{z,\text{ land}} &= -\sqrt{2gh^O_{\max}}, \\ \Delta t^O_{\text{air}} &= \underbrace{\frac{{}^{\mathcal{F}}v^O_{z,\text{ eject}}}{g}}_{\text{ascent}} + \underbrace{\sqrt{\frac{2h^O_{\max}}{g}}}_{\text{descent}}, \end{aligned} \tag{34}$$

else if $({}^{\mathcal{F}}v^O_{z,\text{ eject}} \leq 0)$ then

$$\begin{aligned} h^O_{\max} &= \boldsymbol{r}^{FO}_{\text{eject}} \cdot \hat{\boldsymbol{e}}_{\mathcal{F}3}, \\ {}^{\mathcal{F}}v^O_{z,\text{ land}} &= -\sqrt{\left({}^{\mathcal{F}}v^O_{z,\text{ eject}}\right)^2 + 2gh^O_{\max}}, \\ \Delta t^O_{\text{air}} &= \underbrace{\frac{{}^{\mathcal{F}}v^O_{z,\text{ eject}} - {}^{\mathcal{F}}v^O_{z,\text{ land}}}{g}}_{\text{descent}}. \end{aligned} \tag{35}$$

The planar distance traversed by the occupant in the air, often referred to as the throw distance, is taken as

$${}^{\mathcal{F}}\Delta x^O_{\text{throw}} = \boldsymbol{v}^O_{\text{eject}} \cdot \hat{\boldsymbol{e}}_{\mathcal{F}1}\;\Delta t^O_{\text{air}}, \tag{36}$$

$${}^{\mathcal{F}}\Delta y^O_{\text{throw}} = \boldsymbol{v}^O_{\text{eject}} \cdot \hat{\boldsymbol{e}}_{\mathcal{F}2}\;\Delta t^O_{\text{air}}. \tag{37}$$

The horizontal landing speeds (in the $\hat{\boldsymbol{e}}_{\mathcal{F}1}$ and $\hat{\boldsymbol{e}}_{\mathcal{F}2}$ directions) are equal to their respective horizontal ejection speeds, as air resistance is neglected.

Occupant on Ground We adopt a slide-to-rest model based on the work of Searle [Searle, 1983; Searle, 1993]. We use the occupant's horizontal landing speed, $\| \;{}^{\mathcal{F}}\boldsymbol{v}^O_{s,\text{ land}} \;\|$, the occupant's vertical landing speed, ${}^{\mathcal{F}}v^O_{z,\text{ land}}$, and the coefficient of friction between the ground and the sliding occupant, μ_{slide}, to calculate the occupant's slide distance, from first ground impact to point of rest, viz.,

$$\Delta s_{\text{slide}} = \frac{\left(\| \;{}^{\mathcal{F}}\boldsymbol{v}^O_{s,\text{ land}} \;\| + 0.63\;{}^{\mathcal{F}}v^O_{z,\text{ land}}\right)^2}{2g\mu_{\text{slide}}}. \tag{38}$$

We typically parameterize μ_{slide} to be 0.6 to 0.9. We modify this range as case-specific needs arise; e.g., the occupant slides on ice or some low-friction surface.

The occupant's point of rest is then calculated as the landing position plus the slide distance.

RESULTS

We illustrate the results of our model with a case-specific analysis. As illustrated in Fig. 2, the accident reconstruction depicts a single-vehicle rollover accident, with four complete rolls. It is a left-side-leading roll event. The vehicle's trip, approximate quarter-rolls, and point of rest are indicated. Integer rolls are labeled 0, 1, 2, 3, 4. The ejected occupant's POR is indicated by the dashed circle adjacent to the vehicle's POR. From the accident reconstruction, the distance of the subject occupant's POR from the vehicle's trip point is approximately 325 feet longitudinally (downstream from trip, along the $\hat{\boldsymbol{e}}_{\mathcal{F}1}$ axis) and approximately negative 34 feet laterally (to the right of the trip point, directed along the $\hat{\boldsymbol{e}}_{\mathcal{F}2}$ axis).

Prior to the rollover, the occupant was seated in the vehicle in the 3L position (third row, left seat). From physical

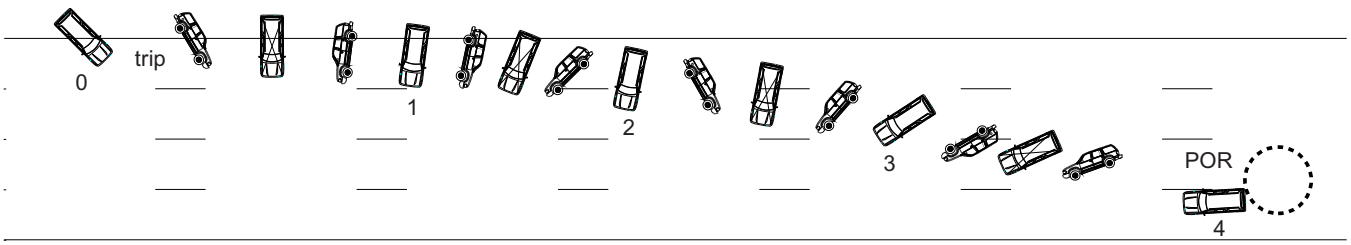

Figure 2: Accident reconstruction diagram in plan view, showing vehicle positions from trip to point of rest (POR) at every approximate quarter-roll. The roll event is left-side-leading (driver-side-leading). Integer rolls are labeled 0, 1, 2, 3, 4. The vicinity of the ejected occupant's POR is indicated by the dashed circle near the vehicle's POR.

Table 1: Case-specific vehicle state variables at discrete locations throughout the rollover event.

point (#)	Δt (sec)	${}^{\mathcal{F}}\Delta s^{V}$ (feet)	${}^{\mathcal{F}}y^{FV}$ (feet)	${}^{\mathcal{F}}\dot{s}^{V}$ (mph)	α (deg)	θ (roll #)	$\dot{\theta}$ (deg/s)	ψ (deg)	$\dot{\psi}$ (deg/s)
0	0	0	0	68.1	0	0	0	-45	0
1	0.309	30.1	0	64.7	0	-0.25	-291	-59	-45.3
2	0.224	20.8	-1.86	62.2	-5.12	-0.5	-402	-90	-139
3	0.207	18.6	-3.35	60	-4.59	-0.75	-434	-97	-33.7
4	0.224	19.3	-4.09	57.5	-2.2	-1	-401	-98	-4.46
5	0.198	16.4	-5.2	55.3	-3.91	-1.25	-455	-102	-20.2
6	0.154	12.3	-6.32	53.6	-5.22	-1.5	-586	-112	-65.1
7	0.173	13.4	-7.43	51.7	-4.78	-1.75	-520	-135	-133
8	0.226	16.7	-10.4	49.3	-10.2	-2	-398	-102	146
9	0.293	20.4	-12.3	46	-5.22	-2.25	-308	-69	113
10	0.255	16.7	-15.2	43.2	-10.2	-2.5	-352	-101	-125
11	0.318	19.3	-17.8	39.8	-7.74	-2.75	-283	-131	-94.5
12	0.327	18.2	-22.3	36.2	-14.2	-3	-275	-147	-48.9
13	0.387	19.3	-28.6	31.9	-19.1	-3.25	-232	-150	-7.75
14	0.346	15.2	-31.2	28.1	-9.83	-3.5	-260	-156	-17.3
15	0.455	17.1	-33.5	23.1	-7.49	-3.75	-198	-160	-8.79
16	2.11	35.7	-43.5	0	-16.3	-4	-42.7	-177	-8.07
Σ	6.2	309.7							

evidence, we know the occupant's ejection portal was the adjacent left, rear cargo window.

We construct the occupant trajectory model in several steps. First, we use case-specific accident reconstruction data to calculate quantities in Table 1 for each known vehicle location—each quarter-roll in this case. These discrete quantities are then interpolated, providing continuous functions for state variables over the duration of the roll event.

The vehicle's roll distance and the vehicle-to-surface friction μ give rise to the vehicle's trip speed, using Eq. (1). Since the accident reconstructionist used $\mu = 0.5$ to construct Fig. 2, we adopt the same value in for our vehicle model to assure consistency of the vehicle's motion. Then, using Eq. (4) and Eq. (5), the vehicle's speed and position are calculated. Knowing the arc-length distance between vehicle templates, the time duration between templates, Δt, can then be calculated. Once time durations over each interval are known, then time-derivative quantities can be determined.

As seen in Table 1, the four-roll event takes 6.2 seconds from trip to rest. The vehicle moves along an arc-length path 309.7 feet in distance. The trip speed is 68.1 mph, and the speed goes to zero at the final point. The negative value of the path angle, α, indicates the vehicle is moving laterally to the right as the rollover progresses.

As seen in Table 1 and Fig. 3, the roll rate magnitude climbs steadily after the trip event to about 400 degrees per second, levels off, then spikes up to almost 600 degrees per second. From the spike, the roll rate decreases until the final vehicle roll configuration. When the vehicle reaches the fourth roll, the roll rate is nearly 45 degrees per second, dropping to zero as the vehicle's suspension brings the vehicle to rest.

The average of the interpolated roll rate magnitude is calculated to be approximately 250 degrees per second, with a single spike approaching 600 degrees per seconds near the 1.5 roll position.

Compared with the roll rates, the yaw rates are signifi-

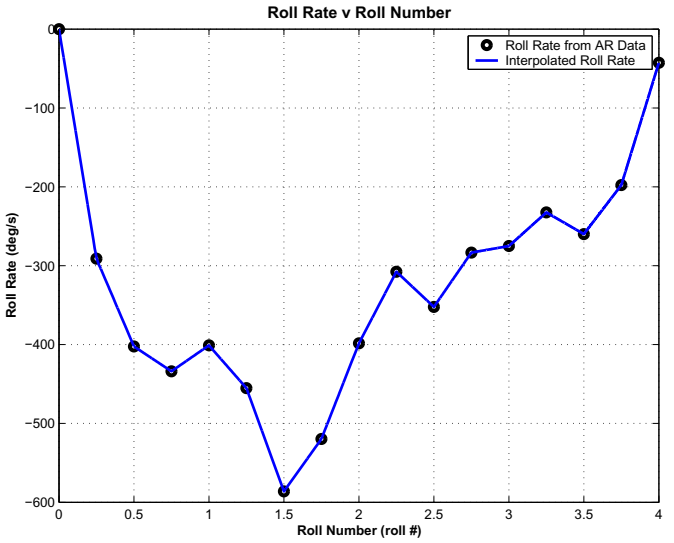

Figure 3: Discrete and interpolated roll rate $\dot{\theta}$ versus roll number.

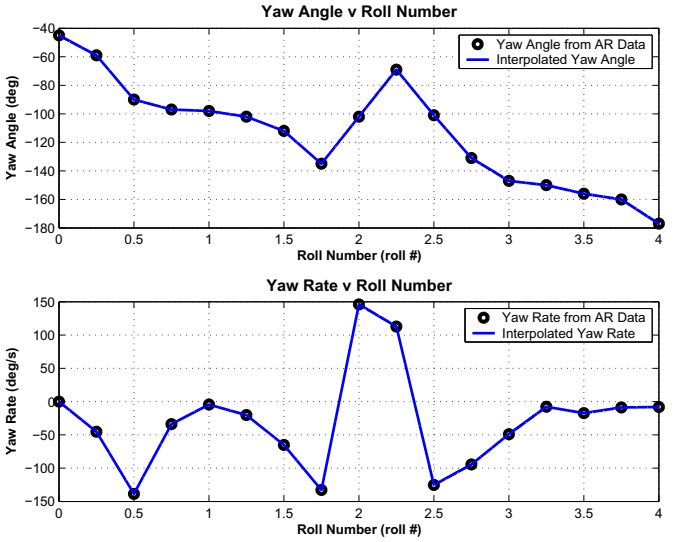

Figure 4: Discrete and interpolated yaw ψ and yaw rate $\dot{\psi}$ versus roll number.

cantly less in magnitude, as seen in Fig. 4. The yaw rates are bounded between ± 150 degrees per second. The average of the interpolated yaw rate is calculated to be approximately -20 degrees per second.

We calculate the occupant landing position and occupant rest position for each admissible ejection time, as a function of roll number, as shown in Figs. 5 and 6. We superimpose the distance from the vehicle's trip to the occupant's actual POR, a constant value indicated with the red dashed line, in both the longitudinal and lateral directions. Possible ejection solutions exist where candidate PORs intercept actual PORs.

Figs. 7 and 8 show the vehicle's position at trip, occupant ejection, and rest. At the ejection point, the path of the ejected occupant is indicated from the vehicle to the ground impact by the first path segment, and from the ground impact to rest by the second path segment. Table 2 shows numeric values for vehicle and occupant positions and speeds for each of the ejection solutions. The occupant launch speed, launch angle β^{O}_{eject}, and maximum height indicate how the occupant was thrown from the vehicle.

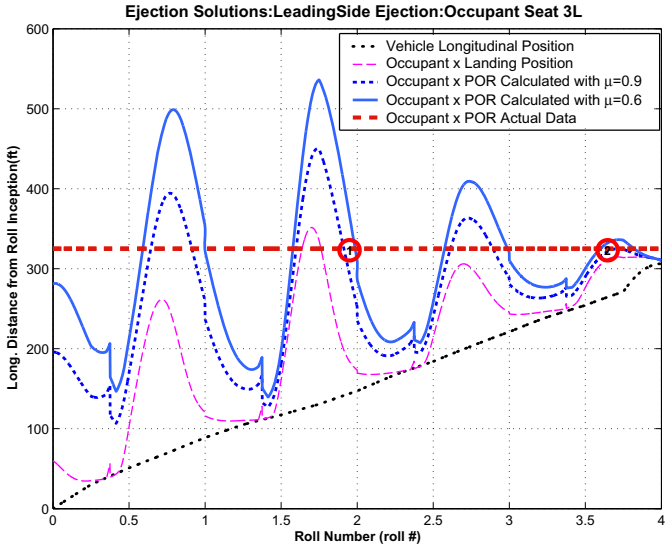

Figure 5: Ejection solutions in the longitudinal direction, $\hat{e}_{\mathcal{F}1}$, as a function of roll number.

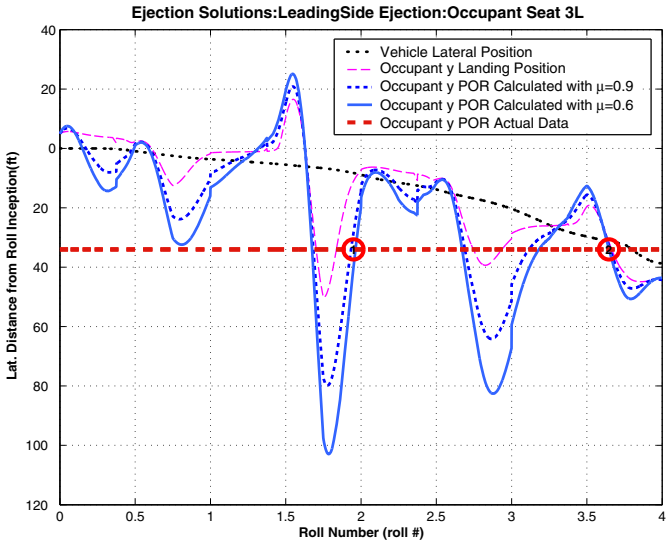

Figure 6: Ejection solutions in the lateral direction, $\hat{e}_{\mathcal{F}2}$, as a function of roll number.

DISCUSSION

The current formulation determines the occupant trajectory following ejection in a rollover accident from a case-specific perspective and incorporates features not included in previously published studies.

Occupant trajectory calculations are based on case-specific accident reconstructions, which provide roll angles, roll rates, yaw angles, yaw rates, positions and velocities for the vehicle over the rollover sequence. By interpolating the known vehicle dynamics at discrete points, we obtain continuous functions of the vehicle kinematics over the rollover.

Table 2: Vehicle and occupant details at each ejection solution—vehicle roll angle, vehicle distance from trip, vehicle speed, occupant ejection angle, occupant ejection speed, occupant vertical landing speed, occupant maximum height, occupant horizontal distance in the air, occupant horizontal distance on the ground, and combined air and ground distance.

solution	θ^V_{eject}	θ^V_{eject}	${}^{\mathcal{F}}s^V_{\text{eject}}$	${}^{\mathcal{F}}\dot{s}^V_{\text{eject}}$	β^O_{eject}	$\| {}^{\mathcal{F}}\boldsymbol{v}^O_{\text{eject}} \|$	$\| {}^{\mathcal{F}}v^O_{z,\text{eject}} \|$	$h^O_{\max}$	Δs^O_{air}	$\Delta s^O_{\text{slide}}$	$\Delta s^O_{\text{air+slide}}$
(#)	(roll #)	(deg)	(feet)	(mph)	(deg)	(mph)	(mph)	(feet)	(feet)	(feet)	(feet)
1	1.95	702	144	50	-6.5	64	-16	6.8	37	147	184
2	3.65	1313	267	25	23	28	-16	8.6	45	15	60

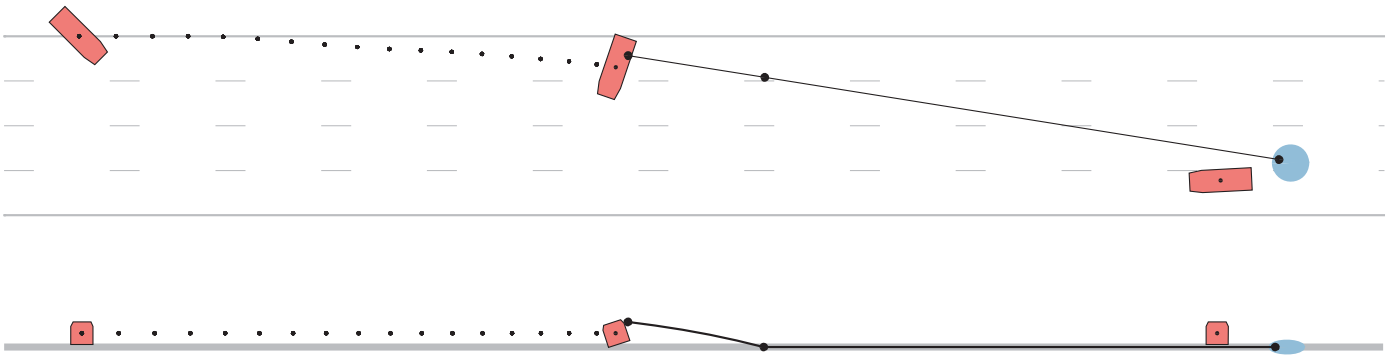

Figure 7: Ejection solution at roll angle θ = 702° (1.95 rolls), top view and quasi-side view, respectively.

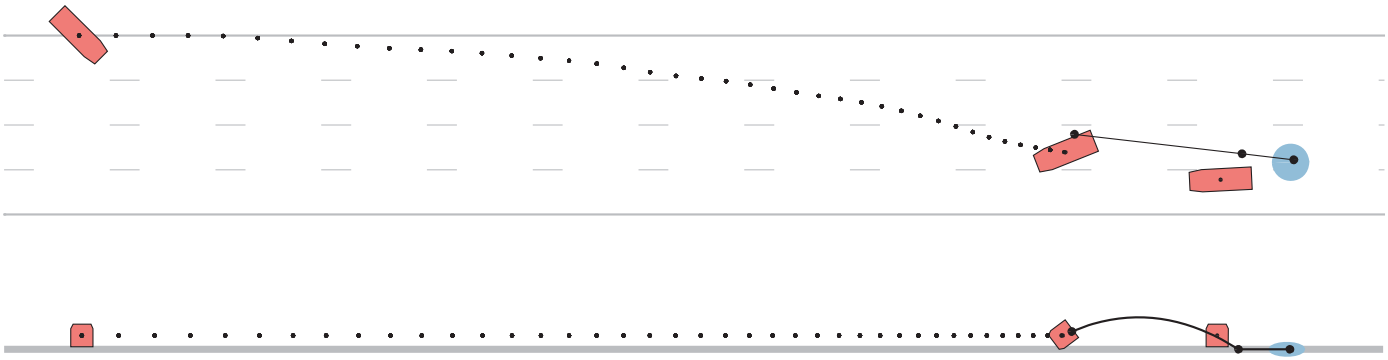

Figure 8: Ejection solution at roll angle θ = 1313° (3.65 rolls), top view and quasi-side view, respectively.

The use of case-specific accident reconstruction data distinguishes the model from existing models that utilize a functional form for the roll rate. The present model makes use of vehicle orientations at times calculated from the accident reconstruction and constructs a roll rate interpolation tailored for each accident event. Such flexibility allows the model to reflect roll rate events in the occupant ejection solutions. A spike, dip, or attenuation in the roll rate at a known time in the rollover is automatically incorporated in the present model. In contrast, existing models may smooth out or miss these effects.

For example, consider a reconstruction where the vehicle ceases rolling and simply translates while sliding on its roof and then resumes a final half-roll to come to rest on its wheels. In this case, the present model, when compared to existing models, would more accurately account for the actual roll rate. Thus, characteristics unique to the accident are captured to the extent that the accident reconstruction is able to predict accurate vehicle orientations and times throughout the rollover.

Care must be exercised when constructing roll and yaw interpolations from the accident reconstruction data. The accident reconstructionist may have limited physical evidence that allows for placement of some, but not all of the vehicle templates on the accident reconstruction diagram. The reconstructionist then may elect to place additional templates on the diagram to illustrate more fully the vehicle's movement throughout the rollover. Such placement should be done judiciously since it becomes manifest in the position and orientation interpolations of the model.

Moreover, these interpolations are differentiated with respect to time to give linear and angular velocities. The interpolations for roll rate and yaw rate, for example, should be reviewed since errors in the position and orientation variables, when differentiated, amplify errors in the linear and angular velocity variables.

It is sensible to check that the roll rate is equal to zero when the roll angle is zero. Not all reconstructionists use the zero roll angle as the beginning of the roll event, how-

ever. A common alternative is a roll angle magnitude of $\pi/8$ for the start of the rollover. In this case, the interpolated roll rate at the beginning of the roll should be nonzero, since the initial roll rate can be estimated from the time elapsed between the zero and $\pi/8$ roll position. The example presented in this paper uses an initial roll angle of zero, as recorded in Table 1; however, the model equally well accommodates inhomogeneous initial conditions.

It is prudent to assure the vehicle roll rate is near zero at the end of the roll event. As seen in Table 1, the example reconstruction, at the final roll position, has a roll rate of -42.7 degrees per second. The physical interpretation is as follows: As the vehicle rolls to rest with a roll rate that goes from -42.7 to zero degrees per second, the vehicle's suspension compresses and dissipates the remaining kinetic energy of the roll.

The use of a constant vehicle drag factor μ, as used in Eqs. (1)–(5), limits this model. It does not account for changes in deceleration that might be caused by hard impacts as corners and edges of a vehicle interact with the ground throughout the rollover. The model may be appropriate if the rollover occurs entirely on the roadway or entirely off the roadway. However, for cases where both on- and off-road portions exist in a single rollover event, and the vehicle-to-ground drag factors for on- and off-road differ substantially, the model may require modification. Changes might be made to create two sub-solutions, one for each of the on- and off-road portions of the rollover event, with care taken to piece together the end conditions from the first portion to the initial conditions of the next portion. Alternatively, since the model uses interpolations for all state variables, the vehicle's speed, given in Eq. (4), could be decomposed into subintervals within $[t_0, t_f]$ and interpolated with different values of μ for each of the subintervals.

The value of the vehicle drag factor provided in the accident reconstruction is the same value we use in the vehicle portion of the present model. This will produce a vehicle speed profile consistent with the speeds calculated in the accident reconstruction. If the accident reconstruction does not provide vehicle translational speeds throughout the rollover, the trip speed, at a minimum, should be verified.

The occupant-to-ground friction coefficient, μ_{slide}, can also introduce limitations. We use a low and a high number to allow for variability of this parameter, and to bound the ejectee's maximum and minimum slide distance. In the present instance, we employed a friction value of 0.6 to 0.9. These values are reasonable compared values found by Funk and Luepke, who calculated the friction coefficient for an articulated test dummy with the ground to be between 0.56 and 1.24, and found a modified average value of 0.66 [Funk, 2007]. Our values are reasonable when compared with work done by others who have studied this topic [Searle, 1983; Searle, 1993; Wood, 2000]. Values of occupant-to-ground should be tailored to meet the underlying physical evidence. For example, in our case work, we used a relatively low friction coefficient for an ejectee who had landed and slid to rest in a freeway median covered with ice plant, a vegetative ground cover that was found to be very slippery.

Candidate ejection times are found by looking at longitudinal occupant travel distances. By matching the point of rest in the longitudinal direction, a series of possible ejection times is obtained. Fig. 5 illustrates the results of the longitudinal analysis for the example presented above. The dotted, black line shows the distance traveled by the vehicle from trip as a function of roll number. The thick, dashed, red line (of constant value) indicates the distance from the vehicle trip point to the point of rest of the occupant in the longitudinal direction. The thin, dashed, magenta curve shows the landing point of the occupant after ejection and subsequent airborne travel. Solid, light blue and dashing, dark blue curves represent the final resting point of the occupant from the trip point of the vehicle for a coefficient of friction of 0.6 and 0.9. The difference between the magenta curve and the blue curves is the ejectee sliding distance after ground impact. Where the blue lines intersect the red line represent the candidate solutions for roll number at occupant ejection.

In this example, there are seven possible ejection points that allow the occupant to reach the point of rest in the longitudinal direction. For the occupant to come to the actual point of rest, the lateral travel distances must also be matched. Only when the longitudinal distance traveled and lateral distance traveled match the occupant's resting position is the solution feasible.

Fig. 6 is analogous to Fig. 5, only with the distances now in the lateral direction. By solving for the lateral travel distance candidate ejection points, several of the seven longitudinal solutions are eliminated. Matching longitudinal and lateral travel distances to the point of rest reduces the possible ejection times to two. We have found that applying a local minimization algorithm to a plot of distance from actual to calculated POR as a function of roll number quickly elucidates a family of feasible ejection solutions. This strategy helped rule out what might appear to be ejection solutions in Figs. 5–6 found by inspection alone. For example, it may appear that a possible ejection solution occurs near the 2 5/8 roll position. Closer investigation through the simple minimization reveals that when the longitudinal solution is met near this roll angle, the lateral solution is too short to be considered feasible.

Table 2 details the vehicle and occupant kinematics for each of the remaining possible two ejection solutions. In the example presented, the vertical impact velocities are identical, but the slide distances are significantly different. The solution possibilities left after accounting for longitudinal and lateral trajectory components can potentially be further narrowed by correlating the occupant injuries with the impact velocities and slide distances associated with

the potential ejection times.

For example, an ejectee presenting with extensive road rash type abrasions may indicate an ejection solution with a large slide distance is more likely than an ejection solution with a small slide distance. An ejectee presenting with crush injuries may indicate an ejection solution where there is post-ejection contact, e.g., the ejectee lands ahead of the vehicle and the vehicle overruns the ejectee.

This model includes the effects of yaw angle and yaw rate as well as fore-aft positioning in the vehicle. These factors influence the travel distance and ejection angle of the occupant. Additionally, the generality of the formulation allows for the analysis of planar vehicular ejection problems where there is no appreciable roll, but significant yaw. The current formulation considers ejection velocity relative to the vehicle, as well. The ejection portal can be any opening in the vehicle–side windows, sunroof, liftgate, windsheild, backlight, or door opening, for example.

Although both roll and yaw dynamics are included in the formulation, the pitch angle and pitch rate effects are not accommodated. Changes in elevation of the vehicle over the roll event and vehicle vertical velocities are not included at this point.

CONCLUSION

We have created a model for occupant ejections from vehicles using case-specific accident reconstruction data. Extending previous efforts, we have included vehicle lateral excursions, vehicle yaw effects, and relative occupant motion within the vehicle. While mathematically more complex than existing models, our new model helps eliminate spurious ejection solutions predicted by simpler formulations. The present work improves our understanding of occupant ejections by advancing the fidelity to the underlying ejection events.

REFERENCES

Aronberg, R., “Airborne Trajectory Analysis Derivation for Use in Accident Reconstruction,” SAE 900367, 1990.

Carter, J.W., Habberstad, J.L., Croteau, J., “A Comparison of the Controlled Rollover Impact System (CRIS) with the J2114 Dolly Rollover,” SAE 2002-01-0694, 2002.

Cooperrider, N.K., Hammoud, S.A., Colwwll, J., “Characteristics of Soil-Tripped Rollovers,” SAE 980022, 1998.

Funk, J.R., and Luepke, P.A., “Trajectory Model of Occupants Ejected in Rollover Crashes,” SAE 2007-01-0742, 2007.

Hovey, C.B., Kaplan, M.L., and Piziali, R.L., “Model for Occupants Ejected from Vehicles with Roll and Yaw,” *American Society of Biomechanics,* August 22–25, 2007.

Orlowski, K.F., Bundorf, R.T., Moffatt, E.A., “Rollover Crash Tests – The Influence of Roof Strength on Injury Mechanics,” *Proc 29th Stapp Car Crash Conference,* paper 851734, 1985.

Parenteau, C., Gopal, M., and Viano, D., “Near and Far-Side Adult Front Passenger Kinematics in a Vehicle Rollover,” SAE 2001-01-0176, 2001.

Searle, J.A., and Searle, A., “The Trajectories of Pedestrians, Motorcycles, Motorcyclists, etc., Following a Road Accident,” SAE 831622, 1983.

Searle, J.A., “The Physics of Throw Distance in Accident Reconstruction,” SAE 930659, 1993.

Thomas, T.M., Cooperrider, N.K., Hammoud, S.A., Woley, P.F., “Real World Rollovers – A Crash Test Procedure and Vehicle Kinematics,” *Proc 12th International Conference on the Enhanced Safety of Vehicles,* pp. 819–825, 1989.

Wood, D.P., “Application of a Pedestrian Impact Model to the Determination of Impact Speed,” SAE 910814, 1991.

Wood, D., and Simms, C., “Coefficient of Friction in Pedestrian Throw,” *Impact,* 9(1):12–15, 2000.

CONTACT

Chad B. Hovey, Ph.D.
Piziali and Associates, Inc.
655 Skyway Road, Suite 202
San Carlos, CA 94070
Telephone: 505-345-2070
Fax: 877-730-6003
e-mail: hoveyc@piziali.com